Electronic Supplementary Material (ESI) for ChemComm.
This journal is © The Royal Society of Chemistry 2017

Supporting Information

Polyoxometalate-Based Gelating Networks for Entrapment and Catalytic Decontamination

*Kevin P. Sullivan,[a] Wade A. Neiwert,[a‡] Huadong Zeng,[a§] Anil K. Mehta,[a] Qiushi Yin,[a] Daniel A. Hillesheim,[a‖] Skanda Vivek,[bΘ] Panchao Yin,[c†] Daniel L. Collins-Wildman,[a] Eric R. Weeks,[b] Tianbo Liu,[c] Craig L. Hill[a]**

Affiliations and current addresses: [a]Department of Chemistry, Emory University, Atlanta, GA 30322, USA. [b]Department of Physics, Emory University, Atlanta, GA 30322, USA. [c]Department of Polymer Science, University of Akron, Akron, OH 44325, USA. †Present address: Chemical engineering and materials division, Oak Ridge National Laboratory, Oak Ridge, TN 37831, USA. ‡ Present address: Department of Chemistry, Bethel University, St. Paul, MN 55112, USA. § Present address: McKnight Brain Institute, University of Florida, Gainesville, FL 32611, USA. ‖ Present address: ABT Molecular Imaging, Inc., Louisville, TN 37777, USA. Θ Present address: School of Physics, Georgia Institute of Technology. Atlanta, Georgia 30332, USA ***Corresponding author. E-mail chill@emory.edu**

Abstract: We report the synthesis and characterization of a new class of organic/inorganic hybrid polymers composed of covalently-bound 1,3,5-benzenetribarboxamide linkers and anionic polyoxovanadate clusters with varying counter-cations. These materials form gels within seconds upon contact with polar aprotic liquids and catalyze the degradation of odorants and toxic molcules under mild conditions, including aerobic oxidation of thiols, hydrogen peroxide-catalyzed oxidation of sulfides and hydroysis of organophosphate chemical warfare agent analogues.

Table of Contents

Materials and Methods (p. 2)
Experimental Procedures (p. 3)
Supplementary Figures S1-S23 (p. 5)
Supplementary Video 1(p. 23)
Results and Discussion (p. 24)
References (p.25)

Materials and Methods

General Instrumentation

All starting materials were used as received unless otherwise specified.

Elemental analyses were performed by Galbraith Laboratories, Inc. (C, H, N) and Atlantic Microlab Inc. (V, Li, Zr).

Infrared (FT-IR) spectra were recorded using a Nicolet TM 6700 FTIR spectrometer Smart Orbit Diamond ATR accessory.

Diffuse reflectance UV/Vis studies were performed using a PerkinElmer Lambda 1050 with 150mm integrating sphere. Spectra were obtained by immobilizing powdered samples on a film and hanging it using a center mount clamp coated in Spectralon® at 0˚.

Z-contrast STEM images were obtained on Hitachi HD2000 scanning transmission electron microscope with 20kV accelerating voltage. TEM images were obtained a Hitachi HD2000 scanning transmission electron microscope at an accelerating voltage of 30kV. Samples were prepared by dispersing **TBA-polyV$_6$** in wet DMF and dropping on Electron Microscopy Sciences CF200-Cu grids, followed by air drying at 40 °C for two days. Contrast enhanced for entire image using Microsoft Word software.

BET isotherms were obtained using a Quantachrome NOVA2000 using N_2 as the adsorption gas.

GC data were obtained using a Hewlett Packard HP 6890 GC system equipped with a HP-5 5% phenyl methyl siloxane column.

XPS measurements were performed using a Thermo K-Alpha XPS. A monochromated aluminum Kα source (1486.6 eV) was used for excitation of photoelectrons. The base pressure of the analysis chamber was 10^{-7} Pa during collection. Survey scan spectra were measured over a pass energy of 200 eV at 1eV energy steps. High resolution scans were performed over a pass energy of 50 eV at 0.1 eV energy steps. Analysis of all spectra were done using CasaXPS software (version 2.3.14). A mixture of Gaussian and Lorentzian functions (GL(X%))were used to fit the high resolution peaks of V, N, and Zr. A reasonable fit was achieved using symmetric lineshapes for V(IV)2p, V(V)2p, N1s, and Br3d. Different GL parameters were used for different elements, but the same parameters were maintained across all measurements. Best fit was achieved using GL(90) for vanadium, GL(56) for nitrogen, GL(30) for oxygen, and GL(80) for bromine. Fitting constraints were applied in such a manner as to be chemically sensible. Doublet peaks for bromide were fit using a separation of 1.05 eV and a ratio of 3:2 between the 3d5/2 and the 3d3/2 peaks; doublet peaks for V(IV) and V(V) were fit using a separation of 7.33 eV and a ratio of 2:1 between the 2p3/2 and the 2p1/2 peaks; doublet peaks for Br were fit using a separation of 1.05 eV and a ratio of 3:2 between the 3d5/2 and the 3d3/2 peaks. V2p was recorded along with O1s, follow up analysis were also performed with a single Shirley baseline across the entire region. O1s peaks were fitted with the assumption that an insignificant amount of adventitious carbon is present on the powdered samples. The stoichiometry of the oxygen species in the linker are preserved in the fit. All measurements were done on dried powders of V_6O_{13} polymers. Samples were standardized against V_2O_5 and TBA(PF_6) powder. All samples were vacuum dried via Schlenk line at 60 °C before introduction into the XPS chamber. The Thermo K-Alpha flood gun was used for charge neutralization during all experiments. Standard deviations of peak fitting parameters were obtained from an analysis of the error matrix generated using a Monte Carlo simulation on the relevant data sets.

Solution ^{31}P NMR spectroscopic measurements were made on a Varian INOVA 600 MHz spectrometer and resonance signals were referenced to 85% H_3PO_4 in H_2O. T_1 = 3.1s, d1 = 15, and no ^{1}H decoupling was used. Solution ^{1}H spectroscopic measurements were made on a Varian INOVA 600 MHz spectrometer.

Solid-state cross-polarization magic angle spinning (CP-MAS) ^{13}C spectra were collected on a BRUKER Avance 600 with ^{13}C frequency of 150.918 MHz and an HCN biosolids probe and MAS speed of 10kHz with 500µs of ^{1}H-^{13}C cross-polarization followed by a Hahn-echo π-pulse of 4µs with 125kHz SPINAL64 ^{1}H (600.13 MHz) decoupling.[1] Dipolar dephasing spectra collected in the absence of ^{1}H decoupling with 50 µs of ^{1}H-^{13}C cross-polarization (Supplementary Fig. 12).

CP-MAS (Figure S8) and Hahn-echo (Figure 1b, Figure S3) ^{13}C (75.48 MHz) spectra were collected on a BRUKER Avance III 300 with an HCN biosolids probe and MAS speed of 13.5 kHz. CP-MAS spectra were collected with 250µs of ^{1}H -^{13}C cross-polarization followed by a Hahn-echo π-pulse of 6µs. Hahn-echo ^{13}C spectra were collected with excitation of all ^{13}C resonances with a 3 µs π/2-pulse followed by a Hahn-echo π-pulse of 6 µs. The relaxation delay for the ^{13}C Hahn-echo spectra was determined by measuring the ^{13}C T_1 with the Torcha method via CP-MAS.[2] All

spectra were collected with 100kHz SPINAL64 ^{1}H (300.13 MHz) decoupling. ^{13}C chemical shifts are referenced externally to TMS using adamantane as a secondary reference.[3]

^{51}V NMR: Solution (157.65MHz) ^{51}V NMR spectrum of **TBA-polyV$_6$**. Spectra were collected on a Varian INOVA 600. 20,000 scans were collected on **TBA-polyV$_6$** gel in DMF for the solution spectrum with a single broad (~15 ppm fwhm) peak at -499ppm. Spectra were processed with 2000 Hz exponential line broadening that matched the signal decay in the FID. Peaks were referenced to $VOCl_3$. The broad peak in the solution spectrum is consistent with reduced motion expected for a gel. Solid-state ^{51}V (78.90 MHz) NMR spectra of **TBA-polyV$_6$** were collected at room temperature with a Bruker 4mm HX magic-angle spinning (MAS) probe and a Bruker Avance III 300 spectrometer. Spectra were measured using a rotor synchronized solid-echo with ^{51}V pulse widths of 1.4µs at multiple MAS speeds (6, 8 and 10 kHz) to identify the center band. Spectra with and without ^{1}H decoupling were identical. Chemical shift is referenced externally to $VOCl_3$ using V_2O_5 as a secondary reference at -609 ppm.[4]

Image analysis for swelling rate (main text Figure 2c and Video S1) was obtained using a Leica DM4500B bright-field microscope equipped with a COHU solid state CCD camera. A 10X objective lens was used. For Video S1, **TBA-polyV$_6$** powder was inserted into a 2mm-diameter capillary tube. Dimethylformamide was added to the tube during video capture. For the analysis of swelling rate for Figure 2c, a sample of powdered **TBA-polyV$_6$** was placed on a glass slide followed by addition of dimethylformamide and particle area was tracked over time. In each case, particle size analysis was conducted using IDL routine methods developed by J. Crocker and D. Grier,[5] and images were processed using ImageJ software.

Experimental Procedures

Chemical Syntheses

Tetrabutylammonium decavanadate ($[(n\text{-}C_4H_9)_4N]_3[H_3V_{10}O_{28}]$) was synthesized according to reported literature procedures.[6] Synthesis of $[(n\text{-}C_4H_9)_4N]_2[(V_6O_{13})[((OCH_2)_3CNH_2]_2$ (**NH$_2$V$_6$**) was also carried out according to reported literature procedures.[7]

Synthesis of $C_6H_3(CONHC(CH_2OH)_3)_3$ (trisBTA). Tris(hydroxymethyl)aminomethane (4.54 g, 37.5 mmol) was dissolved in dry DMA under argon with mild heating. The solution was cooled to 0 °C, followed by the addition of triethylamine (38 mmol). Trimesic acid trichloride (3.32 g, 12.5 mmol) dissolved in dry DMA was transferred dropwise under argon to the solution. The resulting clear, yellow solution was heated to room temperature and was stirred under argon overnight. A yellow/white precipitate was isolated via filtration, concentrated *in vacuo,* redissolved in warm water and stored at 10 °C overnight. The resulting white precipitate (1.34 g, 21% yield) was collected via vacuum filtration. Formation of the product was confirmed by comparisons with literature reports.[8] ^{1}H NMR in DMSO-d_6, ppm (assignment in italics, multiplicity, intensity): 8.25 (C_6H_3, s, 3H); 7.55 (CON*H*C, s, 3H); 4.74 (CH_2O*H*, t, 9H); 3.71 (C*H$_2$*OH, s, 18H). ^{13}C NMR in DMSO-d_6, ppm (assignment in italics): 166 (NH*C*); 135, 129 (C_6H_3); 63 ($HOCH_2$*C*); 60 (HO*C*H_2).

Synthesis of TBA-polyV$_6$. The **trisBTA** linker ($C_6H_3(CONHC(CH_2OH)_3)_3$, 1.00 g, 1.9 mmol) was dissolved in dry DMA under argon with mild heating. Tetrabutylammonium decavanadate ($[(n\text{-}C_4H_9)_4N]_3[H_3V_{10}O_{28}]$, 3.25 g,1.9 mmol) dissolved in dry DMA was transferred to the **trisBTA** solution under argon via cannula. The resulting clear, orange solution was stirred at 80 °C in the dark for one week, resulting in a green gel. The reaction mixture was cooled to room temperature and Et_2O was added, resulting in brown particles in a dark green solution. The solid was purified by repeated swelling in DMF, centrifugation and removal of the green supernatant, followed by contraction in Et_2O and removal of the supernatant. This process was repeated until the decanted liquid was colorless, affording a red solid powder (2.37 g). This was ground into a fine powder using a Wig-L-Bug® instrument, followed by additional swelling and contraction steps until the supernatant was colorless. $[(n\text{-}C_4H_9)_4N]_{2n}[(V_6O_{13})_n[((OCH_2)_3CNHCO)_3C_6H_3]_x[((OCH_2)_3CNHCO)_2((HOCH_2)_3CNHCO)C_6H_3]_y[(OCH_2)_3CNHCO((HOCH_2)_3CNHCO)_2C_6H_3]_z]$ (**TBA-poly$_6$**, x = triply bound linkers, y = doubly-bound linkers, z = singly-bound linkers). Solution ^{51}V NMR (ppm): -501. Solid-state CP-MAS ^{51}V NMR (ppm): -506. Solid-state CP-MAS ^{13}C NMR, ppm (assignment in italics): 166 (NH*C*); 136, 130 (C_6H_3); 84 (VO*C*H_2); 63 ($HOCH_2$*C*); 58 (HO*C*H_2); 54, 25, 20, 14 ($(n\text{-}C_4H_9)_4N$). EA (wt%): C (38.15), H (6.255), N (4.095), V (20.29).

Cation exchange to form Li-polyV$_6$ and Zr-polyV$_6$. A sample of **TBA-polyV$_6$** in a Pasteur pipette containing glass wool at its base was washed with CH_3CN. A solution of 0.1 M $LiBF_4$ in CH_3CN was eluted through the column, replacing the TBA^+ cations with Li^+. To ensure that the exchange was complete, the eluent was collected, evaporated to dryness by rotary evaporation, and dried *in vacuo*, followed by extraction of the $TBABF_4$ with 1,4-dioxane. This solution was filtered, the solvent was removed by rotary evaporation and the resulting solid was dried *in vacuo*. The presence of TBA^+ was confirmed by observing the C-H stretching bands via FT-IR. Elution with the $LiBF_4$ solution was repeated until no C-H stretching bands in the eluent were observed using this method. The resulting product (**Li-polyV$_6$**) in the column was washed with several volumes of CH_3CN to remove excess $LiBF_4$. The same process was repeated using a 0.1 M solution of zirconyl chloride in CH_3CN/H_2O to obtain **Zr-polyV$_6$**. **Li-polyV$_6$**, EA (wt%): C (18.71), H (3.575), N (3.17), Li (1.09), V (25.4). **Zr-polyV$_6$**, EA (wt%): C (11.91), H (1.89), N (3.56), V (16.2), Zr (17.8).

Conditions for Catalytic Reactions

Oxidation of PrSH catalyzed by TBA-polyV$_6$. A sample of **TBA-polyV$_6$** (7.6 mg; 5.4 µmol based on V_6 units) was added to 3.0 mL of 95% DMF / 5% H_2O. The solution was purged with O_2 for 15 minutes, and 1,3-dichlorobenzene internal standard (40 µL, 120 mM) and 1-propanethiol (60 µL, 220mM) were added. The molar ratio was 130 PrSH per V_6 unit. Reactions were monitored by GC analysis of PrSH and PrSSPr. A control reaction was run under the same conditions but without **TBA-polyV$_6$**.

Oxidation of CEES catalyzed by TBA-polyV$_6$ (Figure 4). A sample of **TBA-polyV$_6$** (3.3 µmol based on V_6 units) was added to 1.5 mL of MeOH and was stirred for 1 hour to disperse particles. The 1,3-dichlorobenzene internal standard was added (20 µL), followed CEES (48 µL, 411 µmol). The

zero time point was taken immediately after addition of CEES to the reaction mixture, followed by addition of a solution of 30% w/w H_2O_2 (48 µL, 411 µmol) to initiate the reaction. Conversion to product was monitored by GC analysis of the CEES peak. A control reaction was run under the same conditions but without **TBA-polyV$_6$**. Each reaction was run in triplicate to obtain standard deviations.

The selectivity for 2-chloroethyl ethyl sulfide (CEESO) was determined using ^{1}H NMR of the reaction mixture before and after the reaction. Conditions: 3.3 µmol **TBA-polyV$_6$** (based on V_6 units) was added to a 1.5 mL deuterated methanol (MeOD) and stirred for 1 hour. The 1,3-dichlorobenzene internal standard was added (20 µL), followed CEES (48 µL, 411 µmol). The first NMR aliquot was taken and the ^{1}H spectrum was obtained. After this, a solution of 30% w/w H_2O_2 was added to initiate the reaction. After 40 minutes, the second NMR aliquot was taken and its ^{1}H spectrum was obtained.

Oxidation of CEES catalyzed by TBA-polyV$_6$, Li-polyV$_6$, and Zr-polyV$_6$. A sample of **TBA-polyV$_6$, Li-polyV$_6$, and Zr-polyV$_6$** (3.3 µmol based on V_6 units) was added to 1.5 mL of MeOH and was stirred for 1 hour to disperse particles. The 1,3-dichlorobenzene internal standard was added (20 µL), followed 15 µL 30% aqueous H_2O_2 solution (30% aqueous solution, 140 µmol H_2O_2). Lastly, 16 µL CEES (137 µmol) was added initiate the reaction, and the zero time point was taken immediately after addition of CEES to the reaction mixture. Conversion to product was monitored by GC analysis of the CEES peak. A control reaction was run under the same conditions but without **TBA-polyV$_6$**. Each reaction was run in triplicate to obtain standard deviations.

Hydrolysis of DECP catalyzed by TBA-polyV$_6$. **TBA-polyV$_6$** (3.3 µmol based on V_6 units) was dispersed in 3.0 mL DMF by stirring overnight, then 600 µL of this dispersion was put into a high-pressure NMR tube, followed by addition of 10 µL of diethyl cyanophosphonate (66 µmol) and 50 µL of water (900 µmol) to initiate the reaction. Reaction progress was monitored by ^{31}P NMR. The control reaction was run using the same method but without **TBA-polyV$_6$**.

Hydrolysis of DMNP catalyzed by Zr-polyV$_6$. A sample of **Zr-polyV$_6$** (5 mg, 2.45 µmol based on Zr_4 clusters) was added to a vial containing 1.0 mL aqueous *N*-ethylmorpholine buffer at pH = 10.00 and stirred for 1 hour to disperse the powder. To initiate the reaction, dimethyl *p*-nitrophenylphosphate (DMNP) was added (4 µL, 25 µmol), and reaction progress was monitored by UV/Vis of the *p*-nitrophenolate anion product at 407 nm. Control reactions were run under identical conditions but without the catalyst. Reactions were run in triplicate to obtain standard deviations. Filtration control to test for heterogeneity of the system was done using similar conditions, except all reagents other than DMNP were added to the reaction mixture and were stirred for 2 hours before filtration using 0.2 µm syringe filters. The supernatant was collected and 4 µL (25 µmol) DMNP were added to initiate the reaction.

Gelation Studies

The swelling behavior of **TBA-polyV$_6$** and **Li-polyV$_6$** in various solvents was measured by adding 5 mL of liquid to the solid polymer (~25 mg) and allowing it to gel for 24 hours. Glass wool was inserted into a glass Pasteur pipet to create a filter, and this pipet was weighed. The gel was placed in the pipet and the excess solvent filtered through while the gel was retained on the glass wool barrier. The pipet containing the gel was then weighed to determine the amount of liquid immobilized by the solid gel material. Each experiment was repeated in triplicate to determine the standard deviation.

Supplementary Figures

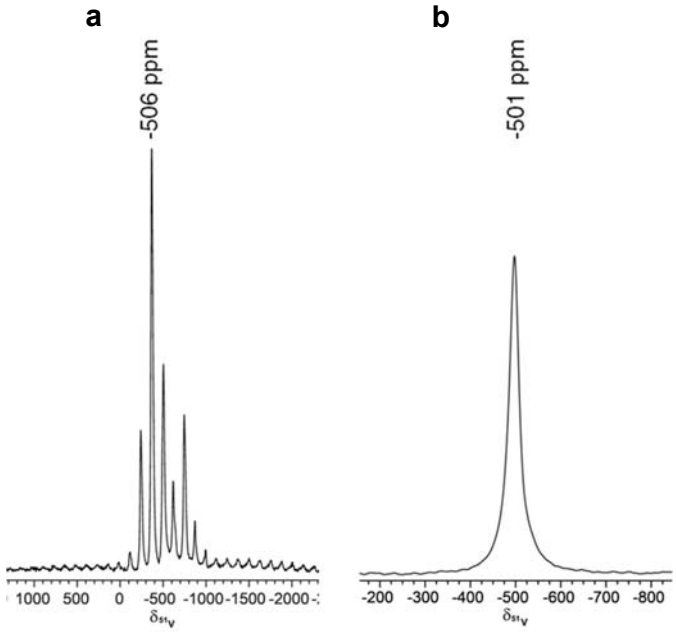

Figure S1. ^{51}V NMR characterization of TBA-polyV$_6$. (**a**) Solid-state magic-angle spinning ^{51}V NMR spectrum of **TBA-polyV$_6$** powder. The center band was located by spinning at multiple magic-angle spinning speeds, indicating the presence of one peak in the spectrum with its associated spinning sidebands. (**b**) Solution ^{51}V NMR spectrum of **TBA-polyV$_6$** in the gel phase when dispersed in *N,N*-dimethylformamide.

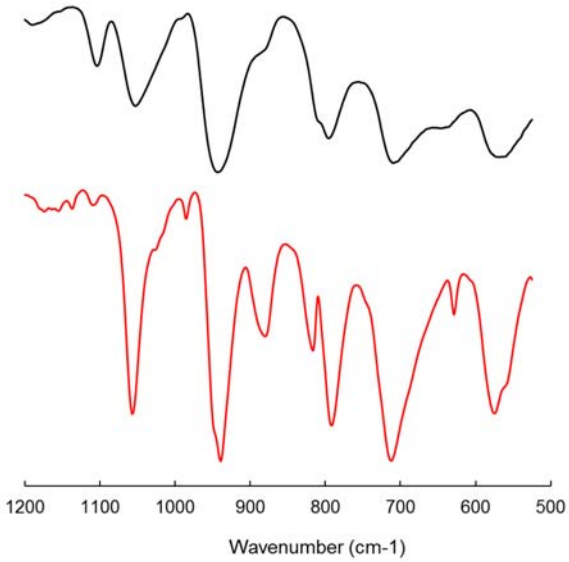

Figure S2. **ATR FT-IR spectra of TBA-polyV$_6$**. **TBA-polyV$_6$** (●) and the known monomeric species **NH$_2$V$_6$** (●). Peaks at 950, 810, 790, 715 are attributed to V-O vibrations.[9] The peaks in the V-O stretching frequency region agree well with reported literature values and with the known monomer **NH$_2$V$_6$**, revealing that the hexavanadate core is intact in **TBA-polyV$_6$**.

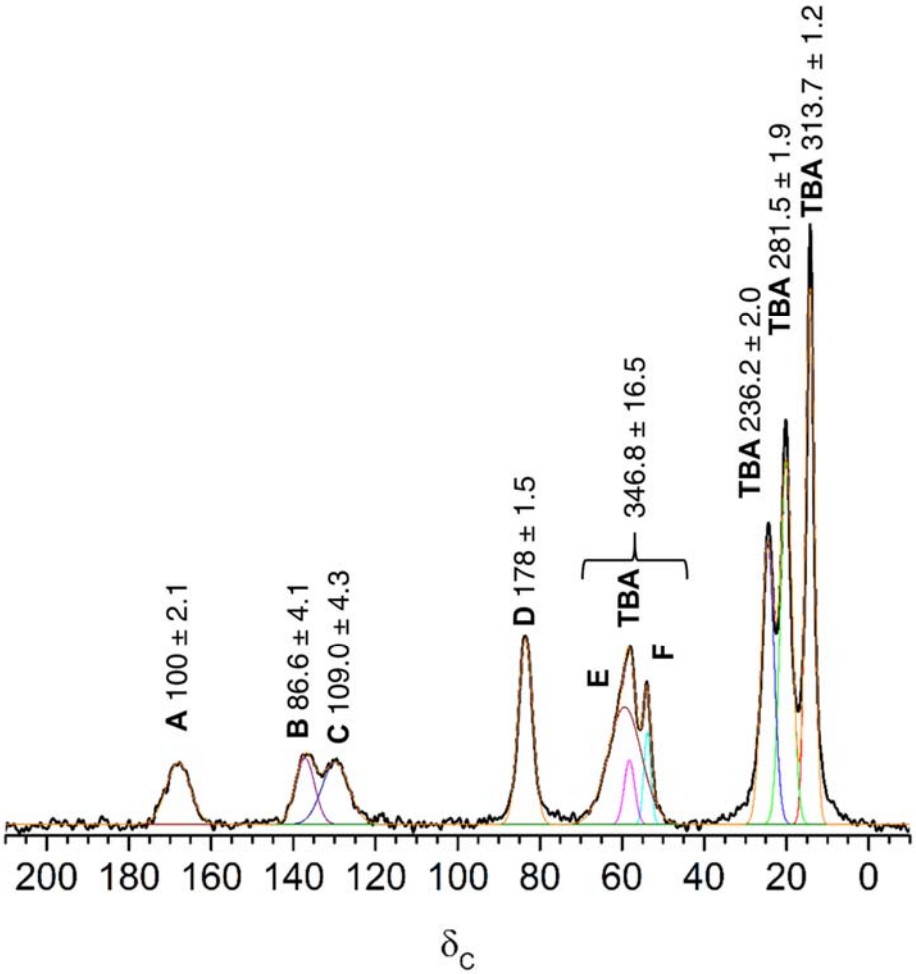

Figure S3. Peak deconvolution of the ^{13}C Hahn-echo natural abundance solid-state spectrum of TBA-polyV$_6$. Direct excitation of the ^{13}C resonances with a Hahn-echo ensures that the spectral intensities are directly related to relative ^{13}C concentration. Due to overlap of the peaks in the 50-70 ppm range, alternate methods were used to ascertain the ratios of the peaks in this region. The ratios of peaks A (amide carbon), B, C (aromatic carbons), and E (quaternary carbon) should be identical based on the molecular structure. We therefore took the average of A, B, and C, and assumed E to be equal to that value (98.53). Additionally, the sum of D (vanadium-bound methylene carbon) and F (unbound methylene carbon) should be equal to three times E. We can therefore solve for the value of F (117.6).

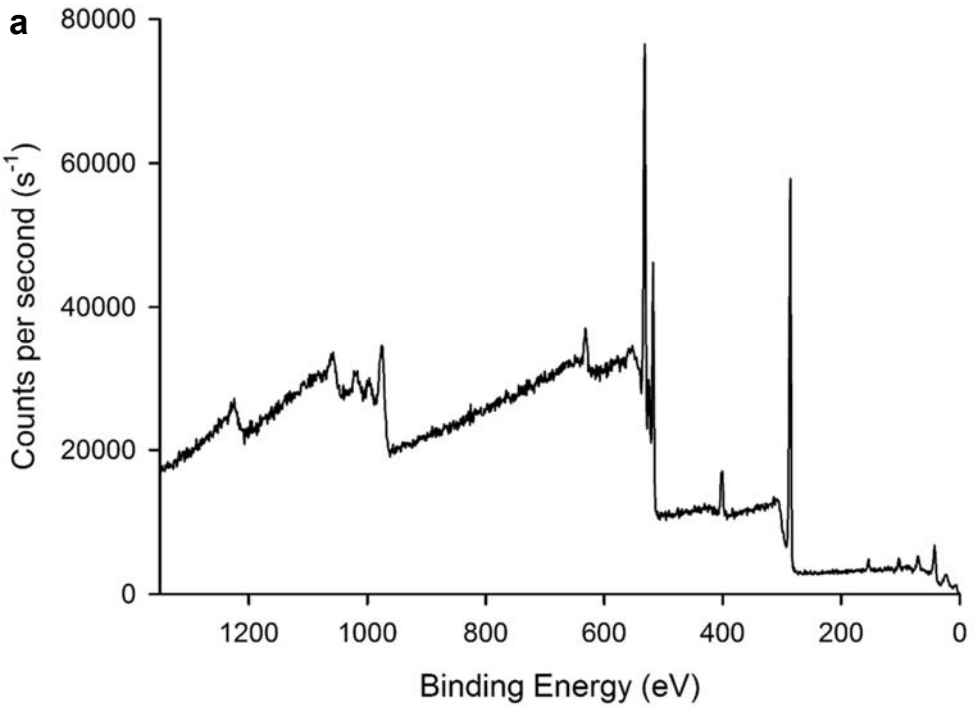
a
80000
60000
40000
20000
0
Counts per second (s-1)
1200
1000
800
600
400
200
0
Binding Energy (eV)

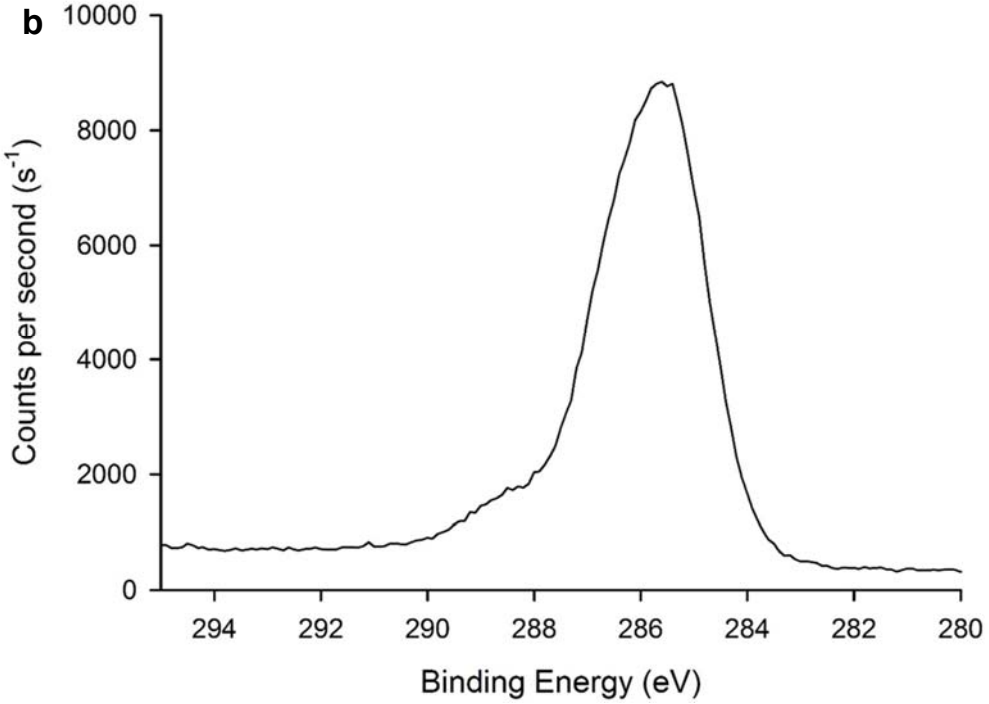
b
10000
8000
6000
4000
2000
0
Counts per second (s-1)
294
292
290
288
286
284
282
280
Binding Energy (eV)

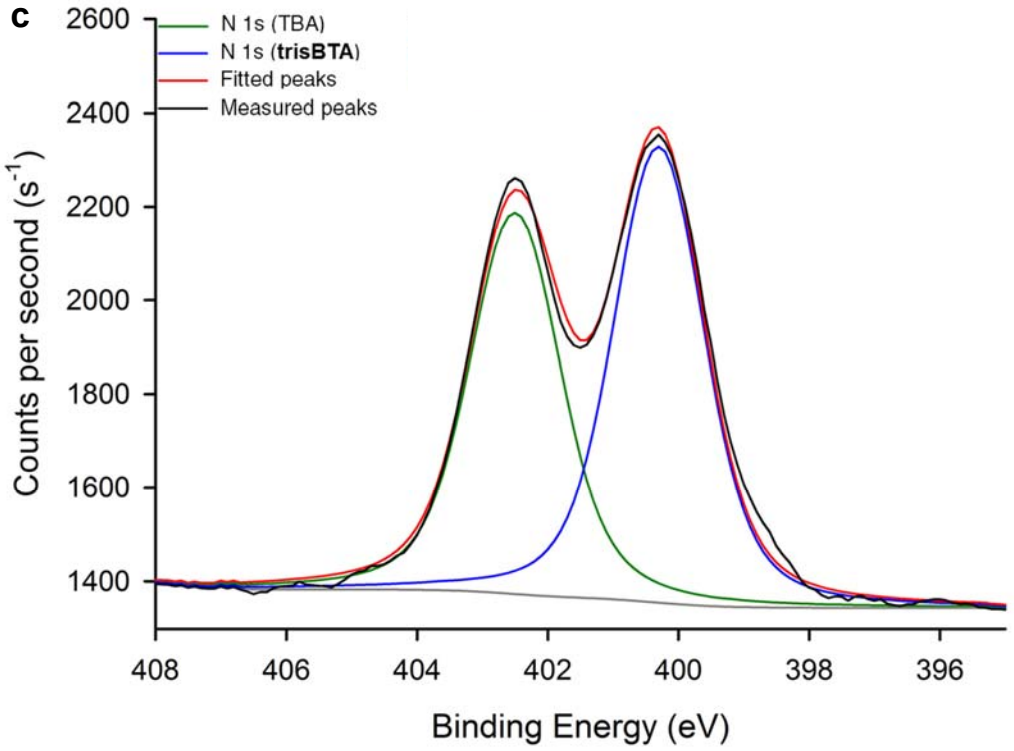
c
N 1s (TBA)
N 1s (trisBTA)
Fitted peaks
Measured peaks
Counts per second (s-1)
2600
2400
2200
2000
1800
1600
1400
408
406
404
402
400
398
396
Binding Energy (eV)

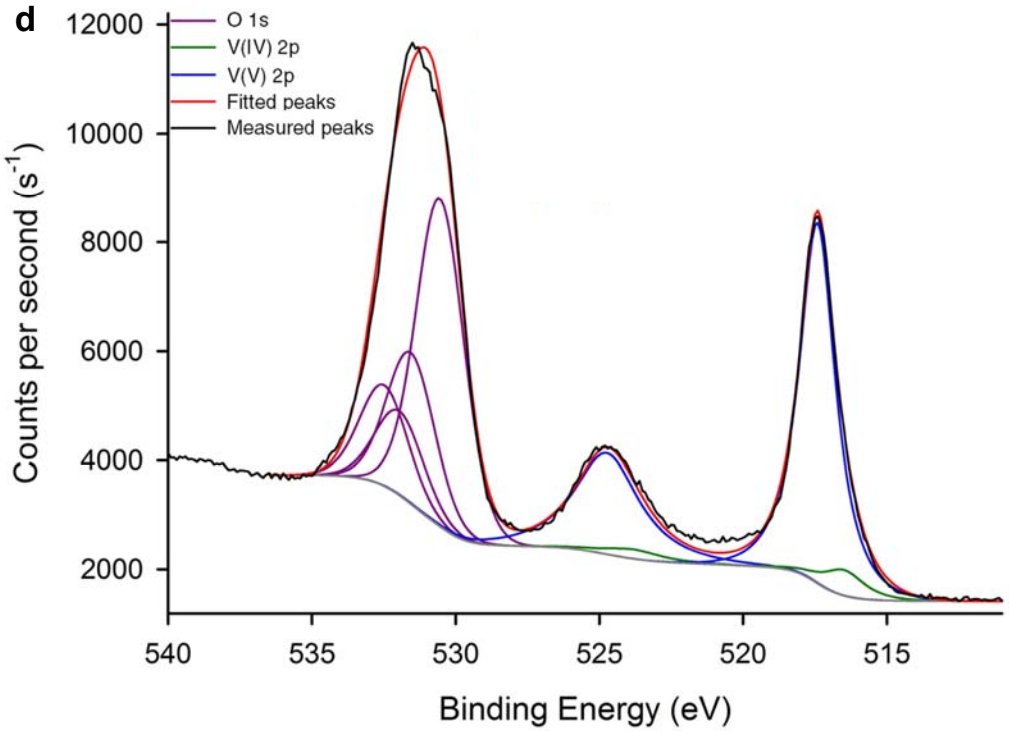
d
O 1s
V(IV) 2p
V(V) 2p
Fitted peaks
Measured peaks
Counts per second (s-1)
12000
10000
8000
6000
4000
2000
540
535
530
525
520
515
Binding Energy (eV)

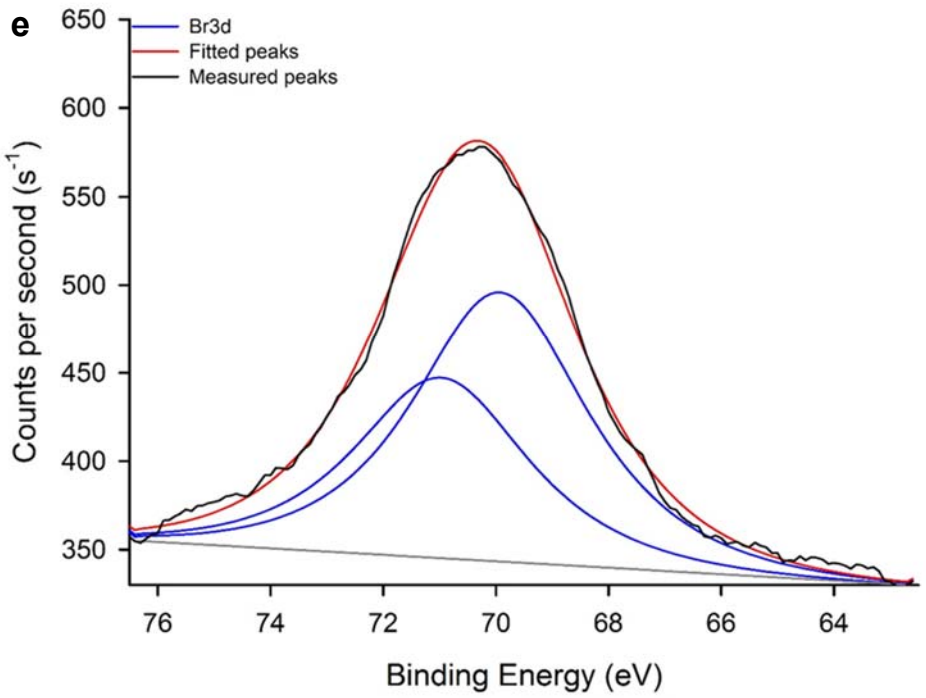

f

Peak	Position (eV)	FWHM (eV)	Area (CPSeV)
Br 3d5/2	69.93±0.05	3.59±0.16	654.24±23.07
Br 3d3/2	70.97±0.05	3.57±0.20	436.16±15.38
N 1s (linker)	400.30±0.01	1.64±0.02	1975.62±28.10
N 1s (TBA)	402.50±0.01	1.64±0.02	1651.32±27.41
V(V) 2p3/2	517.42±0.06	1.49±0.01	12425.11±157.43
V(V) 2p1/2	524.75±0.06	2.65±0.02	6212.56±78.71
V(IV) 2p3/2	516.49±0.06	1.69±0.16	968±147.81
V(IV) 2p1/2	523.82±0.06	2.34±0.20	484±73.91
O 1s (C=O)	531.90±0.06	1.96±0.01	3278.68±7.67
O 1s (VOx)	530.55±0.05	1.96±0.01	12787.9±29.93
O 1s (-OH)	532.50±0.07	1.96±0.01	3934.43±9.21
O 1s (V-OR)	531.56±0.06	1.96±0.01	5901.62±13.81

Figure S4. XPS spectra of TBA-polyV$_6$. (**a**) Survey scan, (**b**) high resolution scan of the C1s region, (**c**) high resolution scan of the N1s region with fitted peak deconvolution (**d**) high resolution scan of the V2p and O1s regions with fitted peak deconvolution (**e**) high resolution scan of the Br3d region with fitted peak deconvolution. (**f**) compilation of data from a-e.

a

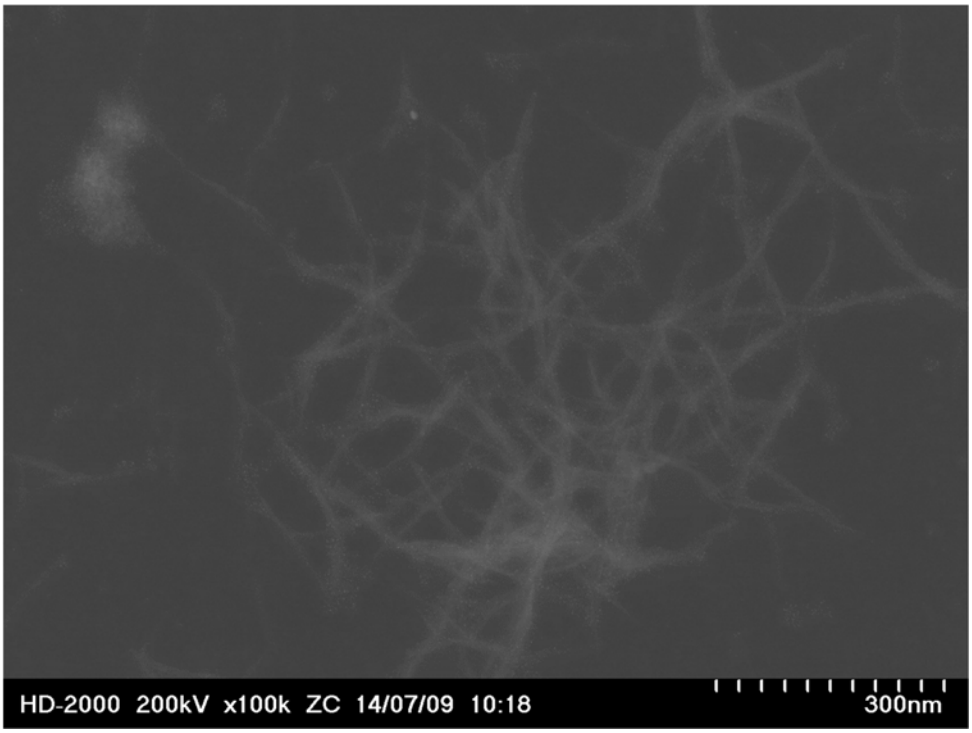
HD-2000 200kV x100k ZC 14/07/09 10:18
300nm

b

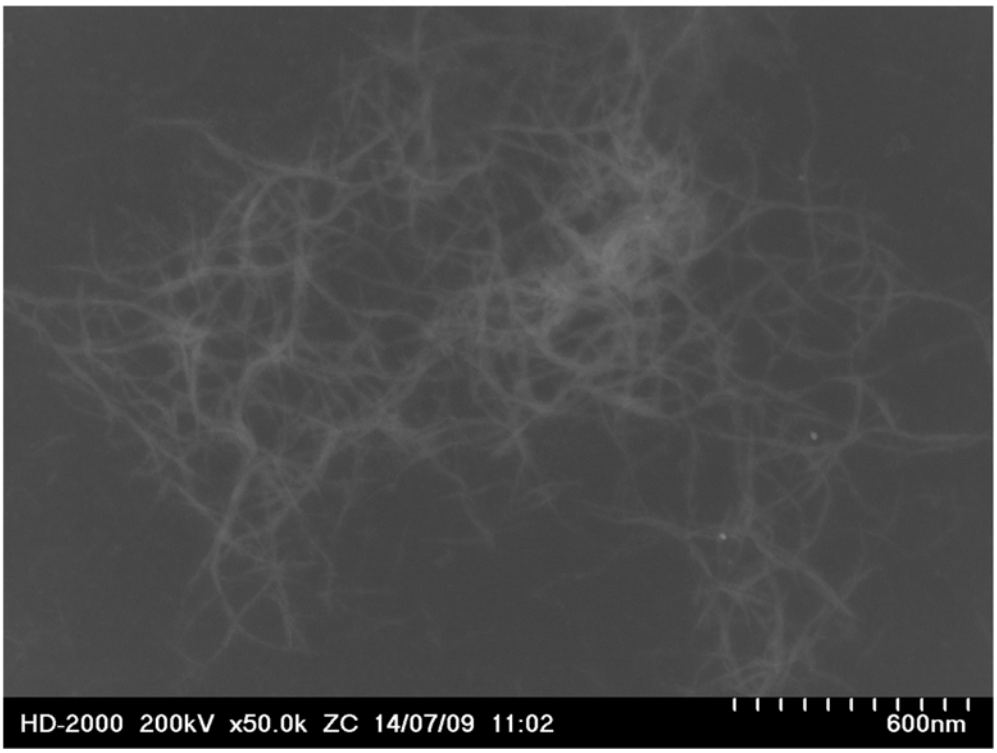
HD-2000 200kV x50.0k ZC 14/07/09 11:02
600nm

c

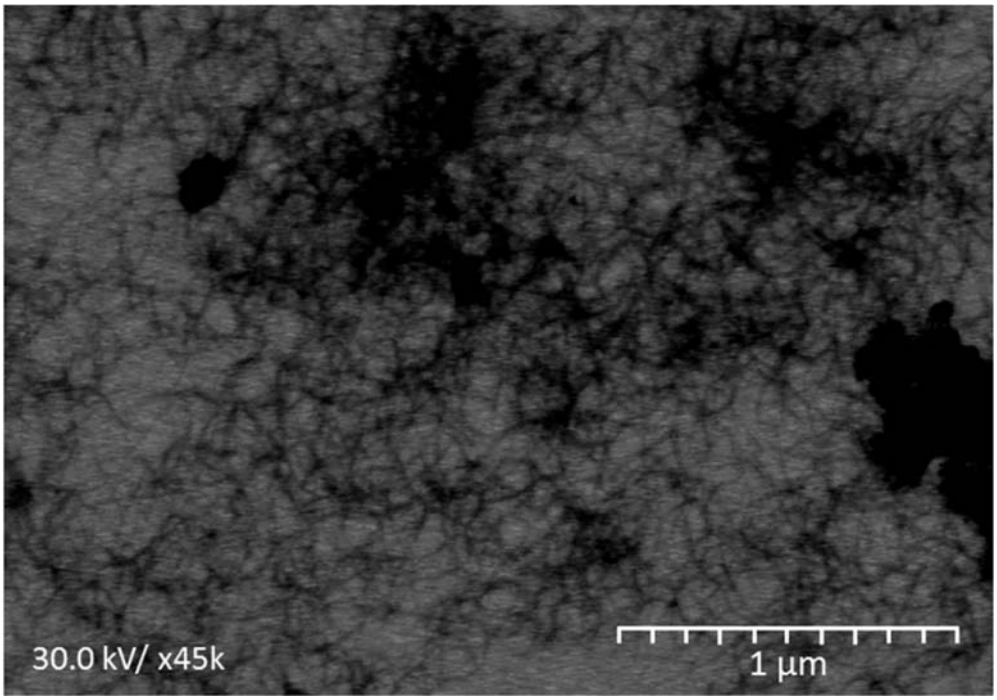

Figure S5. **Electron microscopy of TBA-polyV$_6$.** Images taken after swelling in DMSO and drying under vacuum. Contrast enhanced using Microsoft Word software. (**a, b**) STEM images in Z-contrast mode of **TBA-polyV$_6$**. (**c**) TEM image of **TBA-polyV$_6$**.

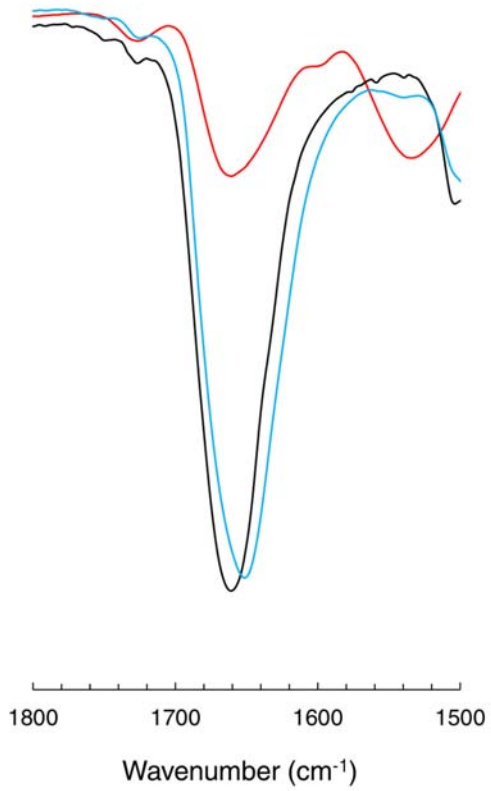

Figure S6. **Hydrogen-bond-induced carbonyl peak shifts**. ATR FT-IR spectra of DMF with varying amounts of **TBA-polyV$_6$** added. The amide 1 band, consisting of the amide C=O stretch, is shown. The peak is observed for pure DMF at 1661 cm^{-1}(●). When 8 wt% gelator is added, a red-shifted amide peak is observed to1652 cm^{-1} (●). This shift is indicative of hydrogen-bonding interactions between the gelator molecules and the DMF carbonyl. This suggests that gelation occurs through formation of hydrogen bonding networks between the N-H hydrogen bond donors in **TBA-polyV$_6$** and the C=O hydrogen bond acceptors in DMF. The spectrum of **TBA-polyV$_6$** (●) alone (no solvent) demonstrates that an increase in the amount of gelator alone is not the cause of the observed red shift in the DMF amide peak.

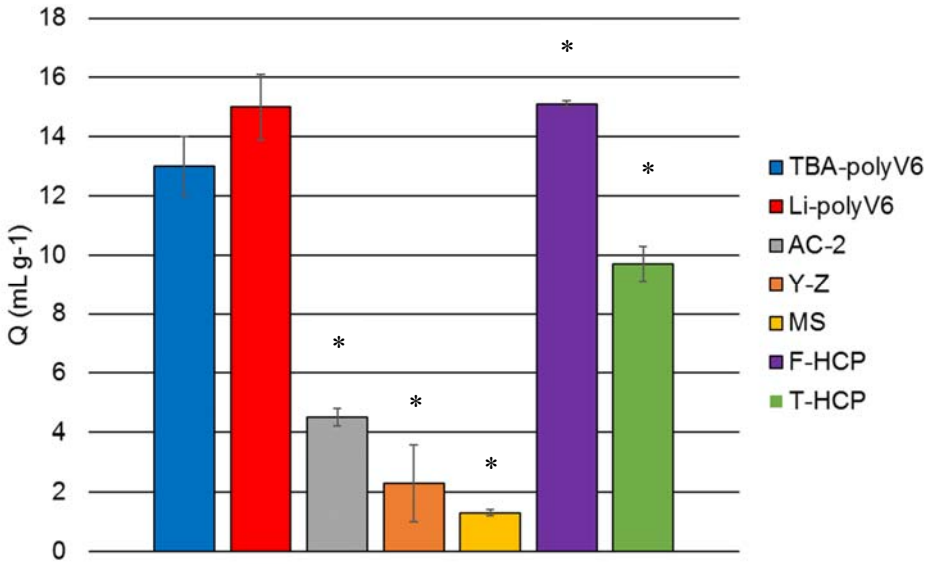

Figure S7. **Comparison of index of swellability (Q) between TBA-polyV6, Li-polyV6 and other adorbents**. Index of swellability for activated charcoal 100-4000 mesh (AC-2), molecular sieves 3Å (MS), γ-zeolite (Y-Z), fluorobenzene-derived highly crosslinked polymer (F-HCP), and toluene-derived highly crosslinked polymer (T-HCP). In each case, the gel was swollen for 24 hours prior to analysis. Data indicated with [*] is from Wilson *et. al*. using similair procedures to determine Q.[10]

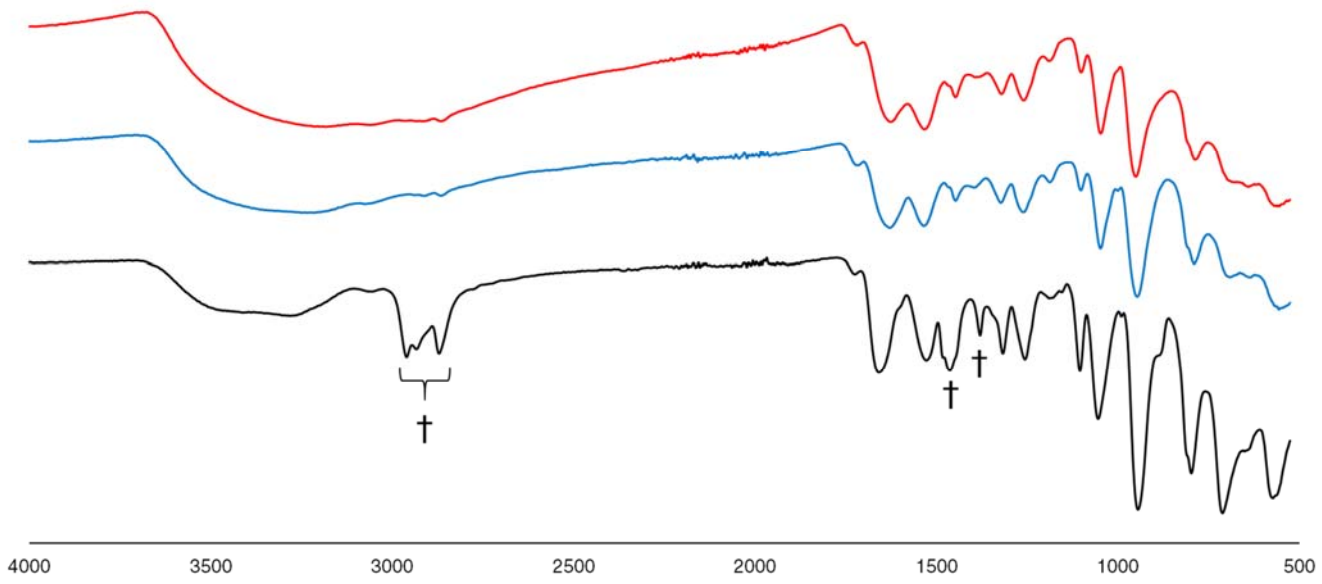

Figure S8. **ATR-FTIR spectra of Li-polyV$_6$ and Zr-polyV$_6$ polymers**. **TBA-polyV$_6$** (●), **Zr-polyV$_6$** (●) and **Li-polyV$_6$** (●). Tetrabutylammonium peaks (†) are present in the **TBA-polyV$_6$** sample at 2930 cm^{-1}, 2950 cm^{-1}, 2870 cm^{-1}, 1490 cm^{-1} and 1390 cm^{-1} but are not present in the cation-exchanged polymers.

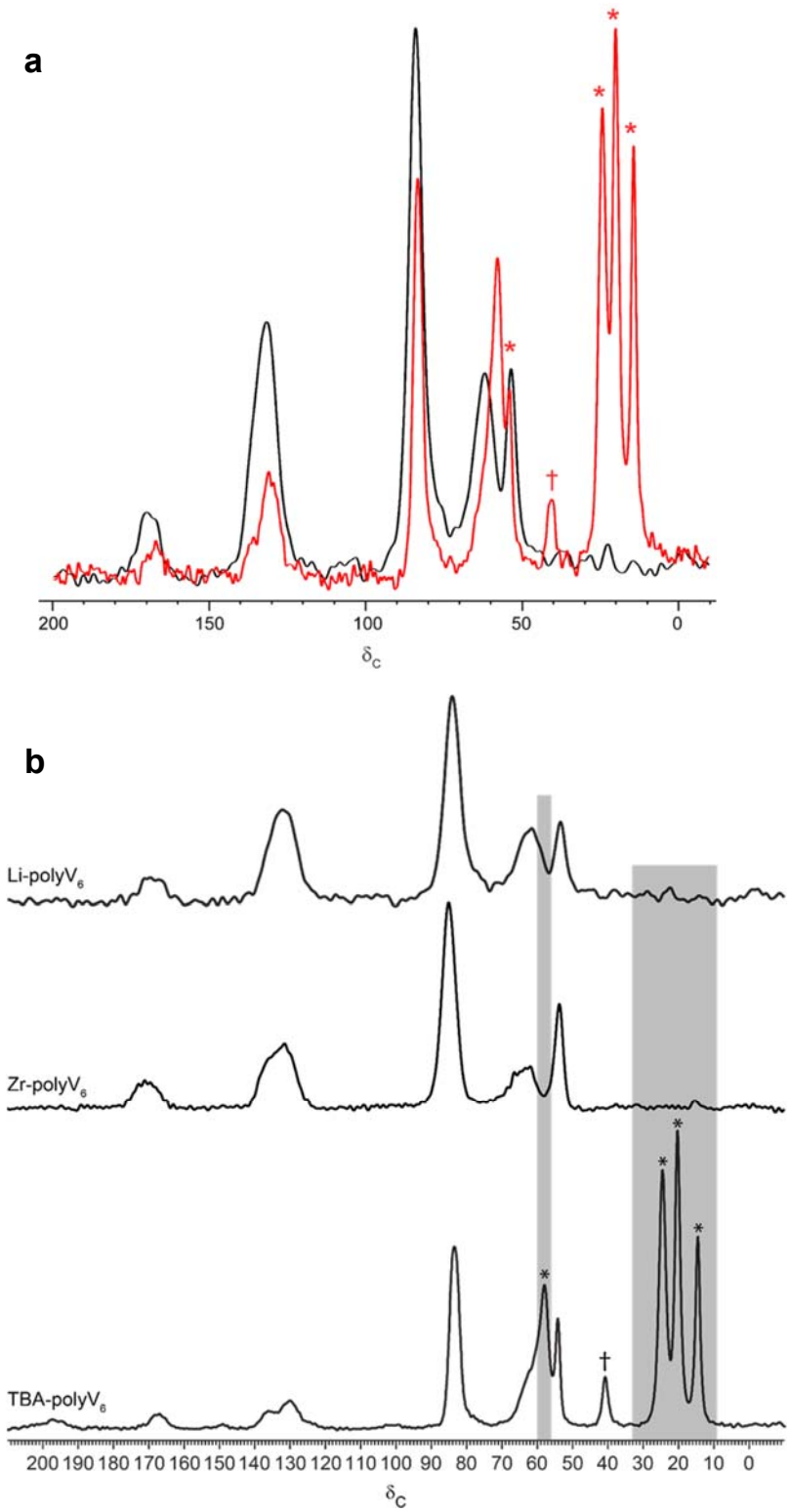

Figure S9. **^{13}C (75.5 MHz) CP-MAS spectra of TBA-, Li-, and Zr-polyV$_6$**. (**a**) **TBA- (●)** and **Li- (●) polyV$_6$** spectra are shown. TBA$^+$ cation (*), and DMSO (†) peaks are indicated. The increased resolution between the triol carbons at 54 and 62 ppm is consistent with distinct H-bonding environments in the **Q-** and **Li-polyV$_6$** samples. TBA$^+$ counter cations are not observed in **Li-polyV$_6$**. (**b**) **^{13}C NMR before and after cation exchange**. ^{13}C (75.5 MHz) CP-MAS spectra of **TBA-**, **Li-**, and **Zr-polyV$_6$**. TBA$^+$ cation (*), and DMSO (†) peaks are indicated.

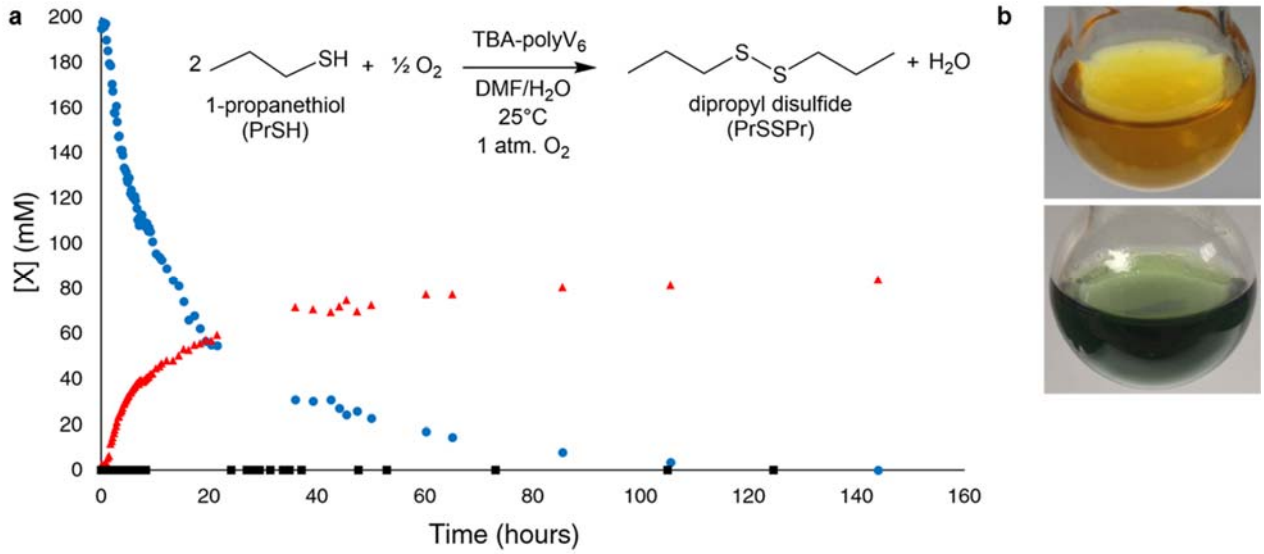

Figure S10. Aerobic oxidation of propane thiol. (**a**) Oxidation of propane thiol (●) to dipropyl disulfide (▲) The mole ratio is 127 PrSH per V_6. A control (■) was run with the omission of **TBA-polyV$_6$**. (**b**) **TBA-polyV$_6$** in DMF before (above) and after (below) addition of PrSH.

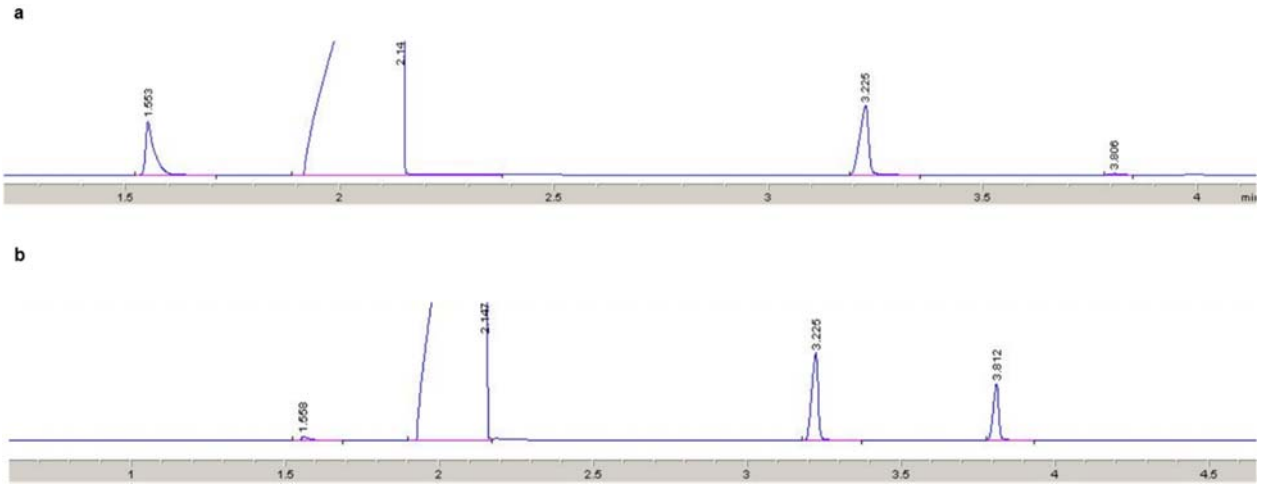

Figure S11. Gas chromatography peaks for propane thiol reaction. (**a**) GC peaks taken from near the start of the catalytic reaction and (**b**) GC peaks taken at the end of the catalytic reaction. Propane thiol (1.5 min elution time) is converted to dipropyl disulfide (3.8 min elution time). DMF (2.1 min elution time) and the internal standard 1,3-dichlorobenzene (3.2 min elution time) are also shown.

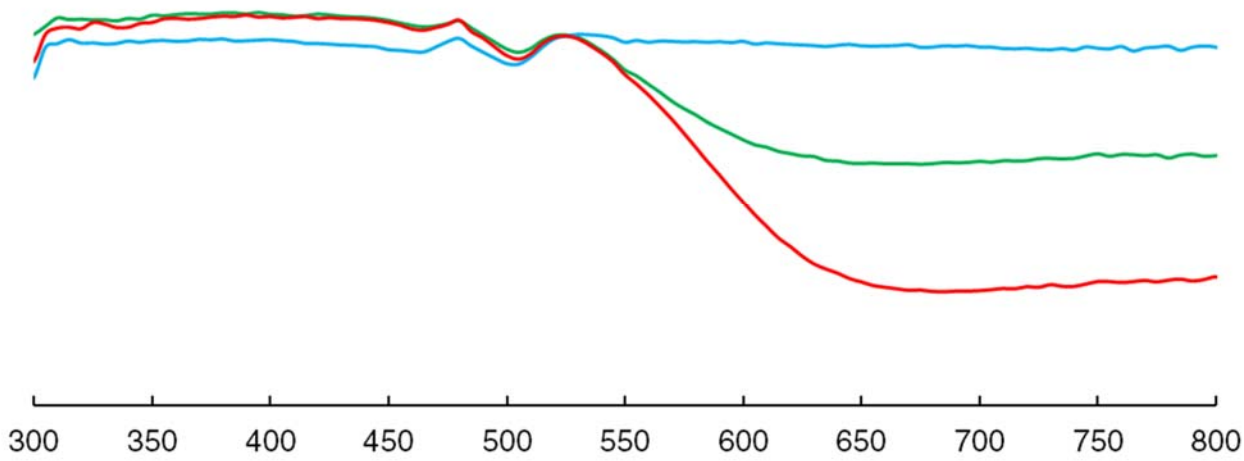

Figure S12. Diffuse reflectance UV/Vis spectra of TBA-polyV$_6$. Sample of **TBA-polyV$_6$** before (●) and after (●) reduction by excess ascorbic acid, resulting in a very broad peak arising from IVCT bands in the region from 600-1000 nm. Upon addition of PrSH (●), reduction of the V_6 center results in a green color, consistent with reduction of V_6 sites within the material.

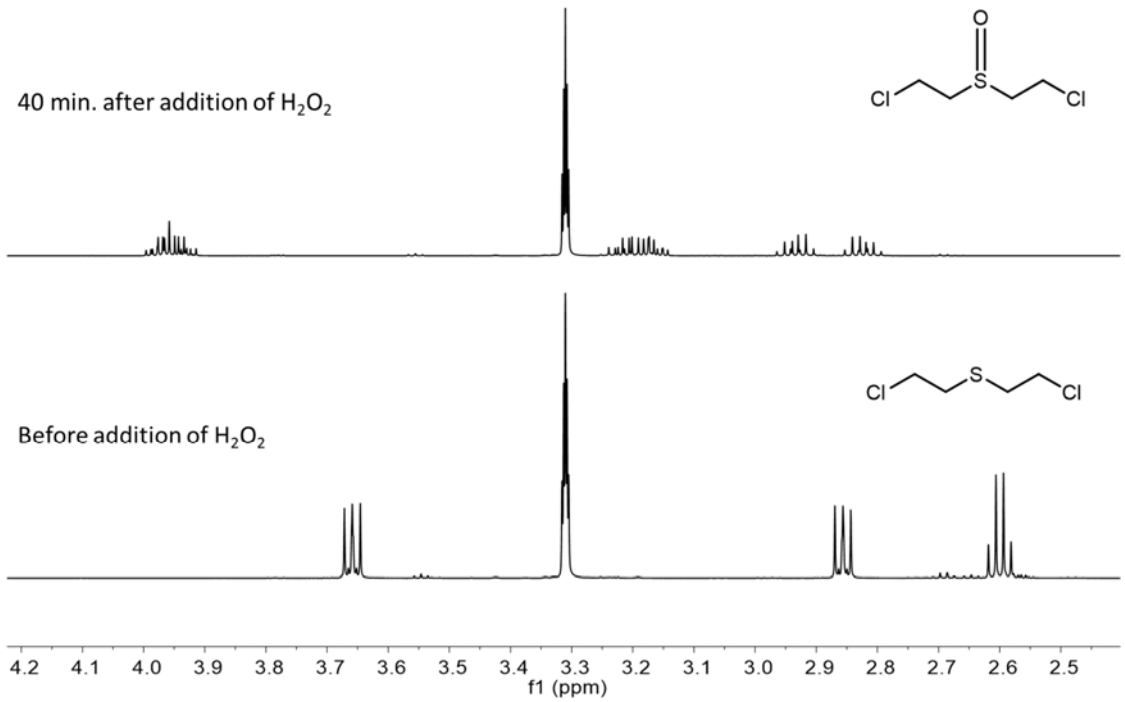

Figure S13. ^{1}H NMR used to determine speciation. ^{1}H NMR of reaction mixture before (below) and after (above) completion of the catalytic reaction, demonstrating near-quantitative conversion of CEES to CEESO without the formation of $CEESO_2$.

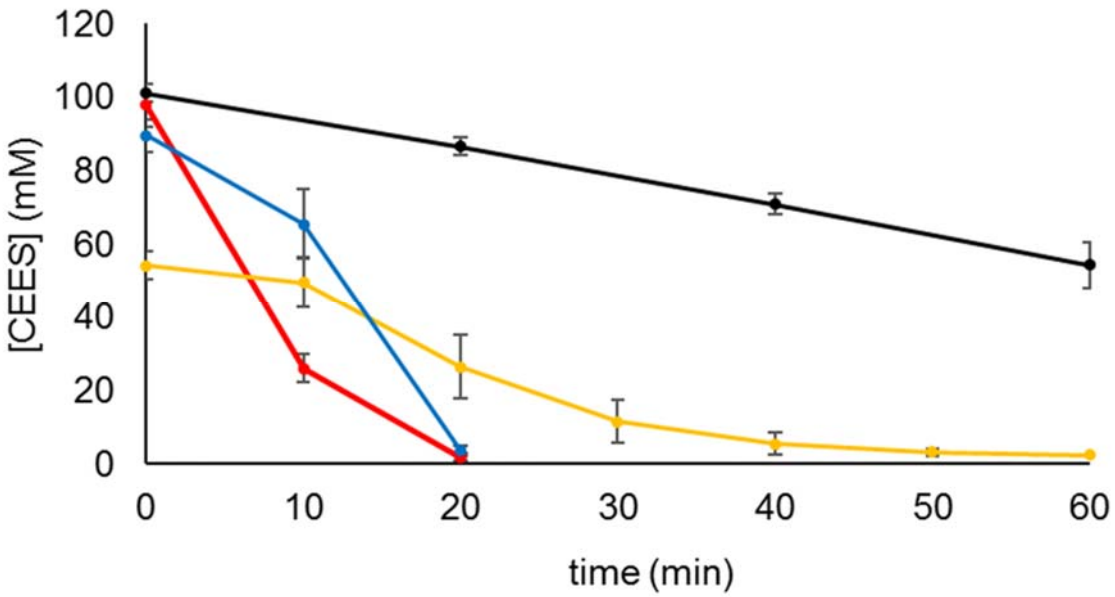

Figure S14. CEES sulfoxidation by H_2O_2 and polyV$_6$ **polymers**. The mole ratio of the catalyzed reaction was 1 V_6: 40 CEES: 40 H_2O_2 in all cases. The uncatalyzed control reaction (●) was run with the omission of **TBA-polyV$_6$**. Reactions were repeated in triplicate and error bars are reported. **TBA-polyV$_6$** (●), **Li-polyV$_6$** (●), and **Zr-polyV$_6$** (●) reactions are shown. Interestingly, the reaction using **Zr-polyV$_6$** as the catalyst initially shows a very rapid oxidation of ~50% of the CEES, followed by slower kinetics to achieve complete conversion.

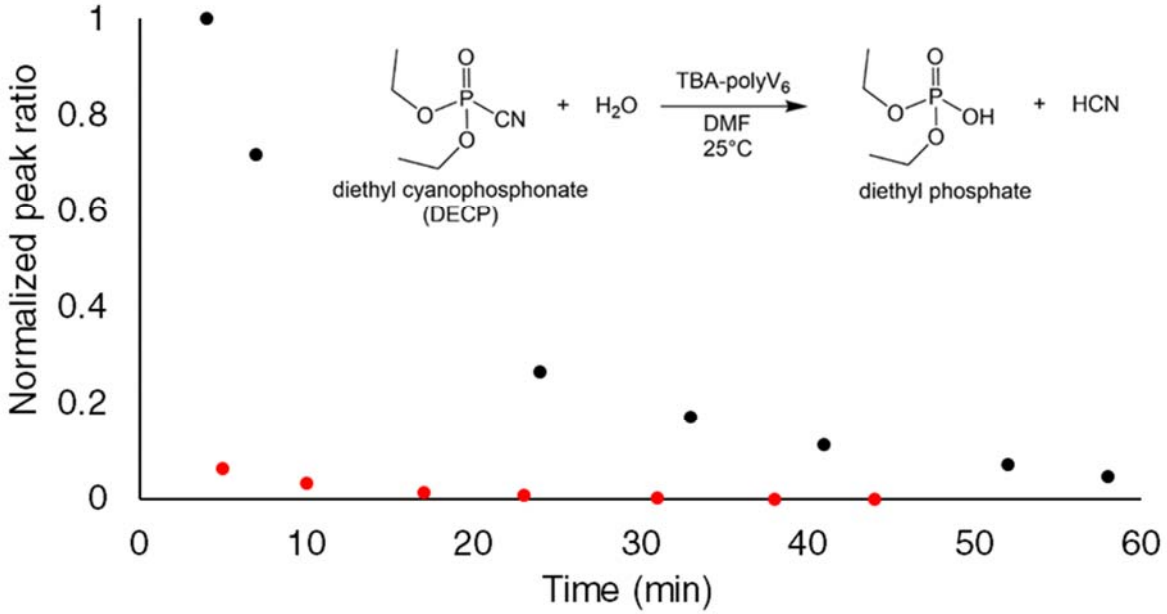

Figure S15. Hydrolysis of DECP catalyzed by TBA-polyV$_6$. Hydrolysis of diethyl cyanophosphonate (DECP) catalyzed by **TBA-polyV$_6$** in DMF. The DECP: **TBA-polyV$_6$** molar ratio was 20:1 based on V_6 units. Reactions were monitored by ^{31}P NMR. The control reaction (●) was run using the same conditions as the catalyzed reaction (●) but with the omission of **TBA-polyV$_6$**.

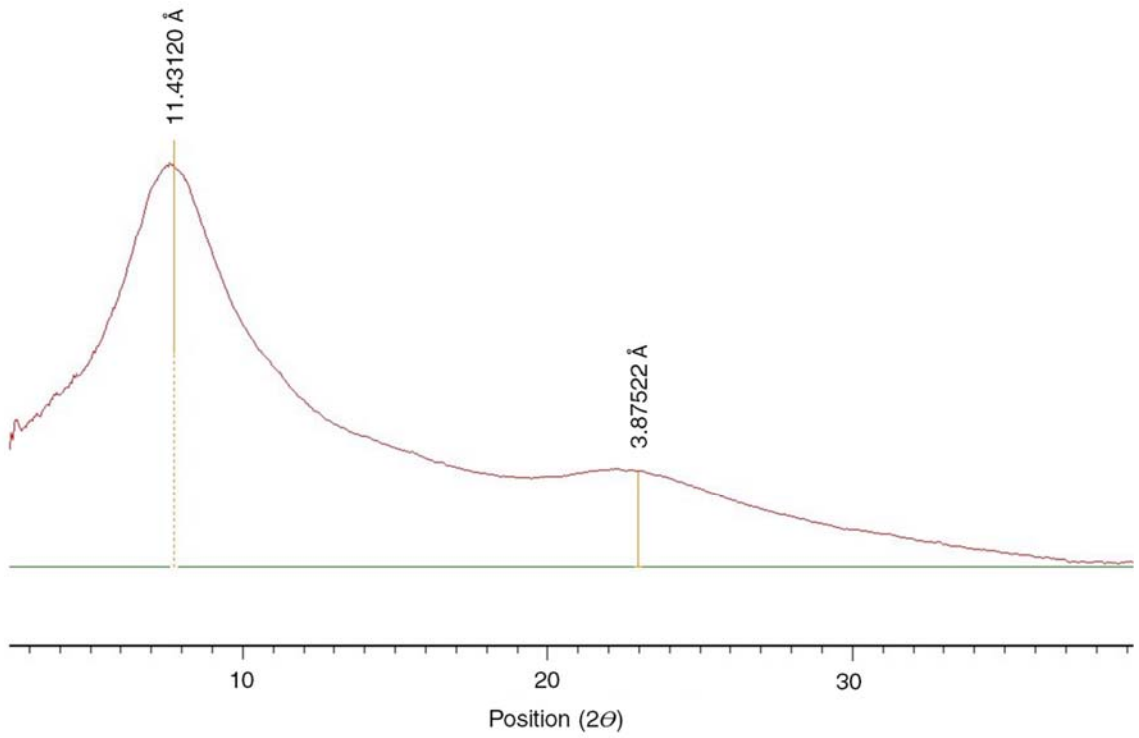

Figure S16. Powder X-ray diffraction (PXRD) of TBA-polyV_6. Distances are indicative of local ordering of V_6 clusters within the material. Measurements were obtained using a D8 Discover powder X-ray diffractometer with VANTECH detector. A Kryoflex X-ray generator with a Co sealed tube running at 1.4 kW (35 kV, 40 mA) of power output provided the X-ray radiation.

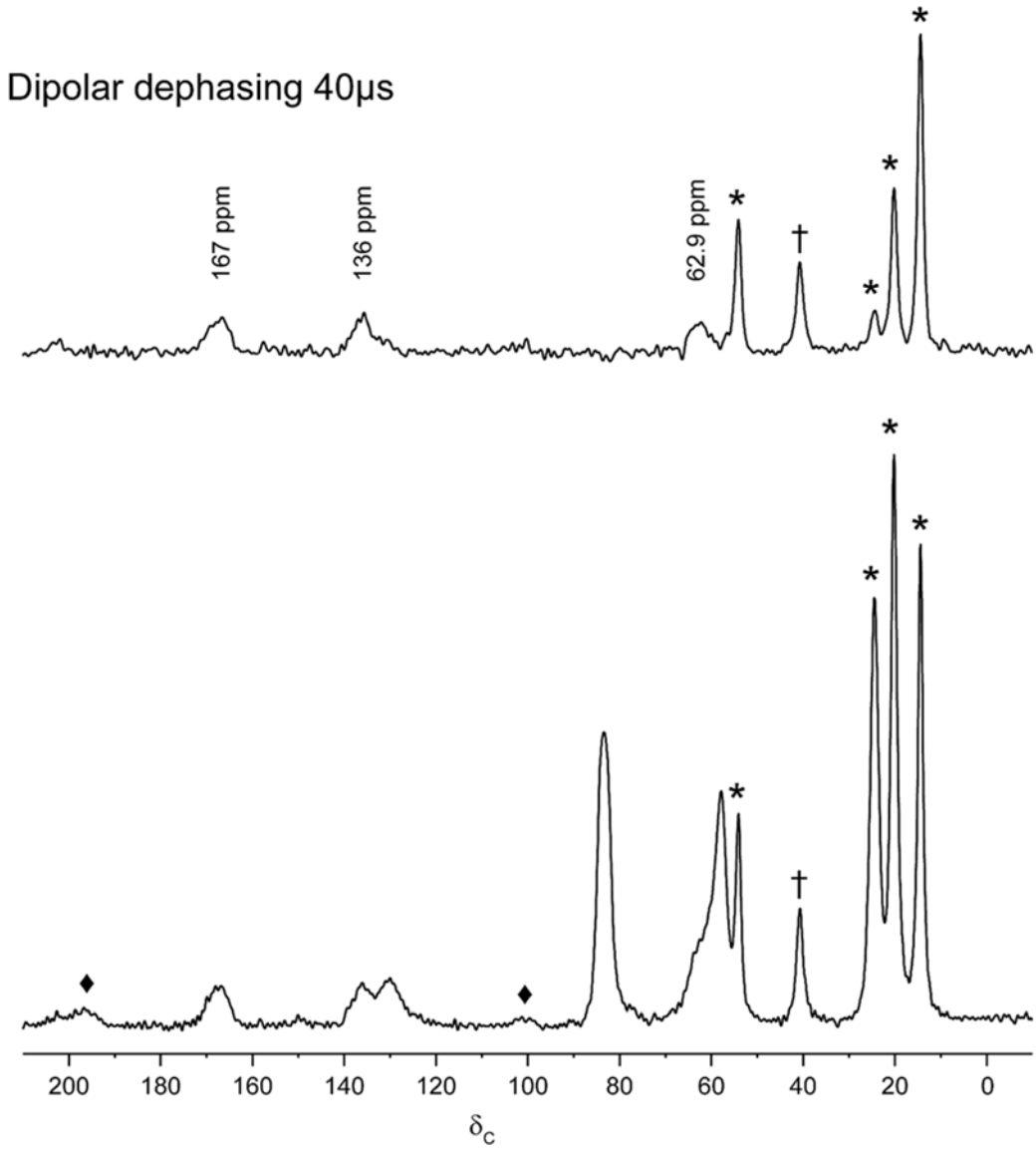

Figure S17. Dipolar dephasing ^{13}C solid-state NMR spectra. ^{13}C (150.9 MHz) spectra of **TBA-polyV$_6$** (bottom) without and (top) with 40µs dipolar dephasing. TBA peaks in the dipolar dephased spectrum are consistent with motional averaging of the ^{13}C-^{1}H dipolar coupling. The resonance at 167 ppm is assigned to the amide carbon, the resonance at 136 ppm is assigned to the non-protonated aromatic carbon of **TBA-polyV$_6$** and 62.9 ppm resonance to the quartenary carbon of the triol. TBA cation (*), DMSO (†), and spinning sideband (◆) peaks are indicated.

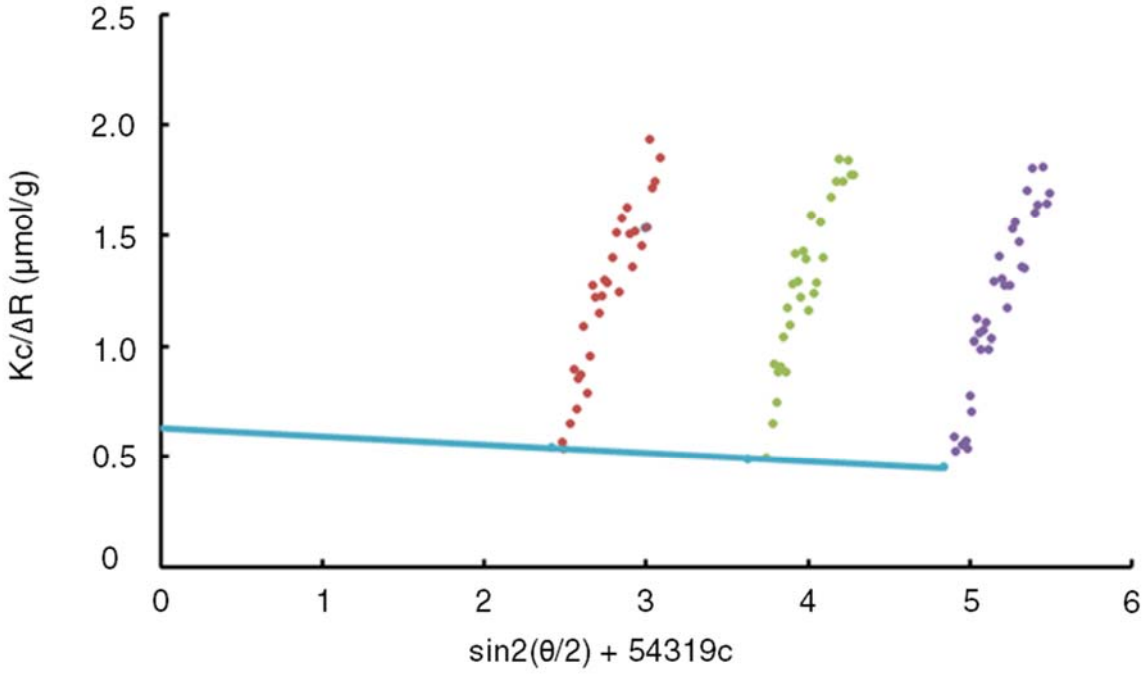

Figure S18. **Static light scattering of TBA-polyV$_6$**. Zimm plot of the static light scattering measurements of the solutions of **TBA-polyV$_6$** in DMF/water mixed solvent (85% DMF/15% H_2O). The solution of **TBA-polyV$_6$** was prepared by dissolving 1.8 mg of **TBA-polyV$_6$** in 20 mL DMF/water mixed solvent (vol. % 85/15). The solid hybrid sample was fully dissolved after the solution was put in 70 °C oven overnight. The solution was then filtered and used as stock solution. Solutions with concentrations from 0.01 mg/mL to 0.09 mg/mL in the mixed solvent were prepared. The dn/dc for the hybrid in the mixed solvent was determined to be -0.112 mL/g within the above concentration range. SLS experiments were performed at scattering angles (θ) between 30 and 100°, at 2° intervals. Solutions with concentrations of 0.90 (●), 0.68 (●), and 0.45 (●) mg/mL were used. Derived from Rayleigh-Gans-Debye equation [11], a Zimm plot was used to analyze the SLS data to obtain the molecular weight of the hybrid. The average molecular weight was determined to be (1.586±0.033)*10^6 g/mol. Data were obtained using a commercial Brookhaven Instrument LLS spectrometer equipped with a solid-state laser operating at 532 nm.

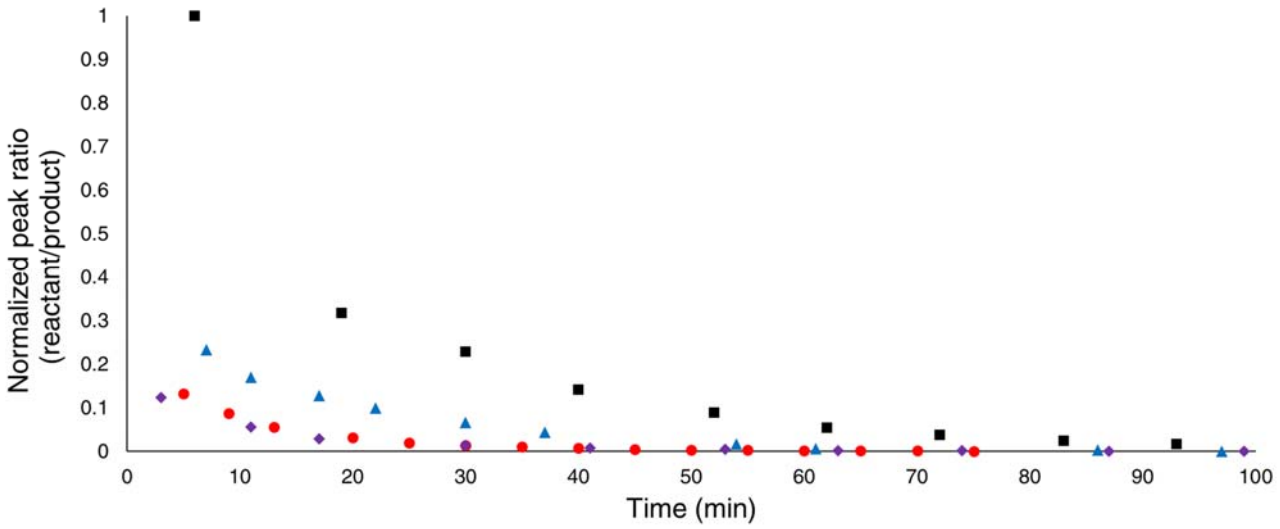

Figure S19. Hydrolysis of diethyl cyanophosphonate (DECP) catalyzed by linker and monomer. **trisBTA** linker (▲, 11 µmol) and the monomeric **NH_2V_6** (◆, 5.4 µmol). The **trisBTA** linker enhances the hydrolytic rate. The monomer exhibits a similar rate of hydrolysis to **TBA-polyV$_6$** (●, 3.9 µmol based on V_6 units). The control reaction (■) was run identical conditions as the catalyzed reaction but with the omission of **TBA-polyV$_6$**.

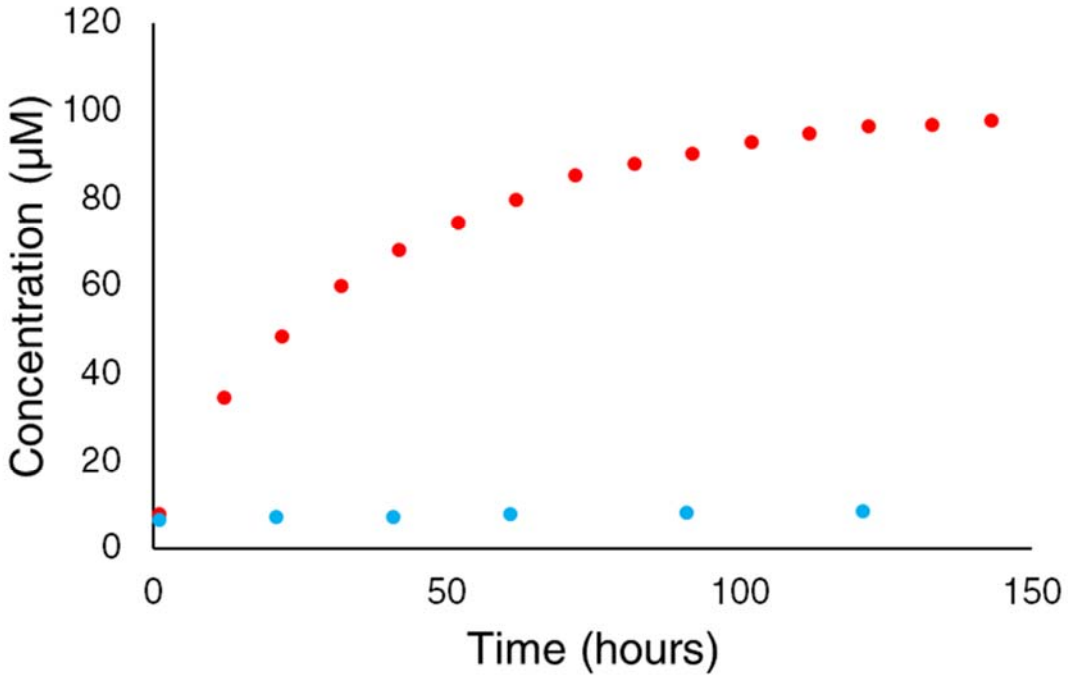

Figure S20. **Hydrolysis of dimethyl *p*-nitrophenylphosphate (DMNP) catalyzed by Zr-polyV$_6$**. **Zr-polyV$_6$** (5.0 mg, 2.45 µmol) and 4 µL (25 µmol) DMNP were added to aqueous 0.45M *N*-ethylmorpholine (NEM) at pH 10 (●). Reactions were monitored by UV/Vis spectroscopy, detecting the formation of the 4-nitrophenolate hydrolysis product. To ensure a heterogeneous reaction, 5.0 mg of **Zr-polyV$_6$** was stirred in 0.45M NEM buffer at pH = 10.00 for two hours, followed by filtration using 0.2 µm syringe filters. The supernatant was collected and 4 µL DMNP were added to initiate the reaction, which exhibited negligible activity (●).

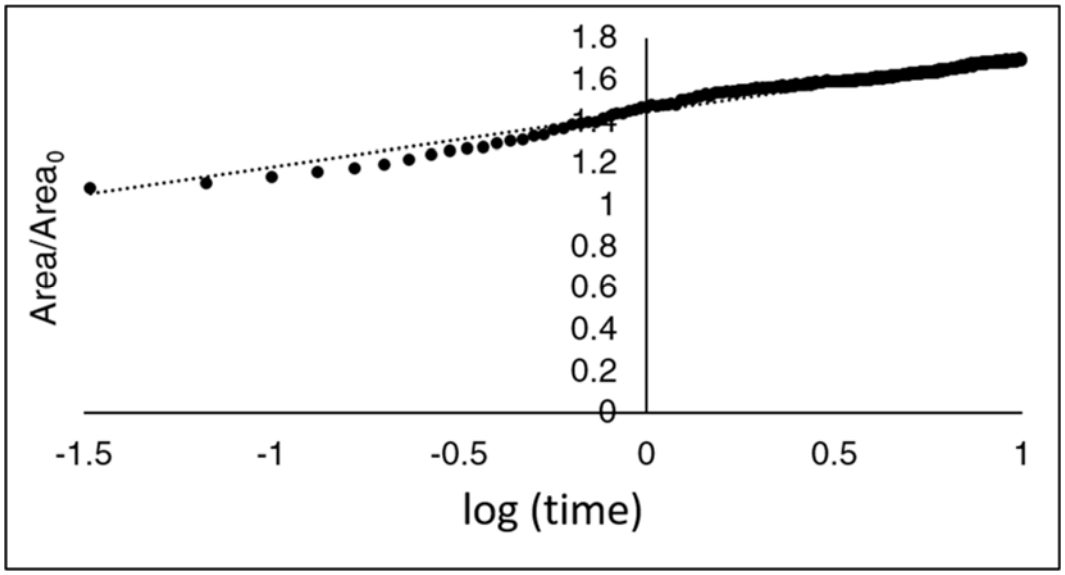

Figure S21. Log plot of the swelling data from Figure 2c. The semi-log plot is roughly linear, suggesting exponential swelling kinetics.

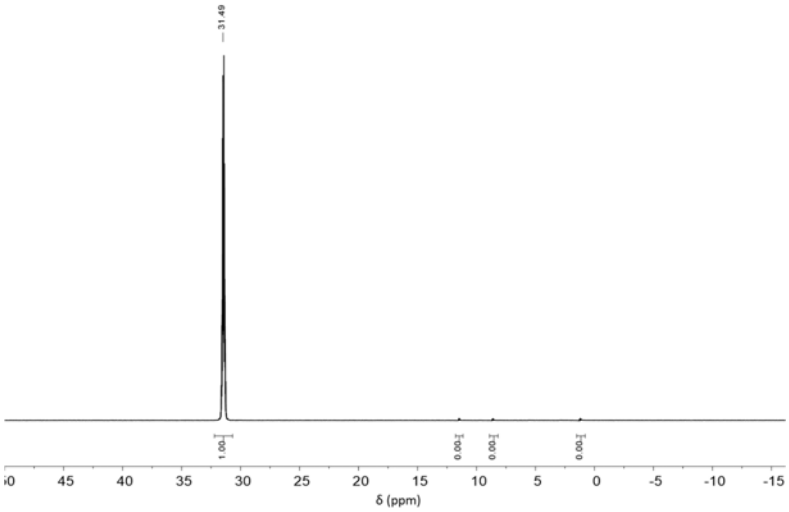

Figure S22. ^{31}P NMR of DMMP after exposure to TBA-polyV$_6$ for 24 hours. To confirm that **TBA-polyV$_6$** does not react with DMMP after exposure for 24 hours during the gelation experiments, we added 20 mg **TBA-polyV$_6$** to a vial containing 300 µL DMMP and obtained the NMR spectrum after 24 hours demonstrating that negligible conversion to products occurred over this time.

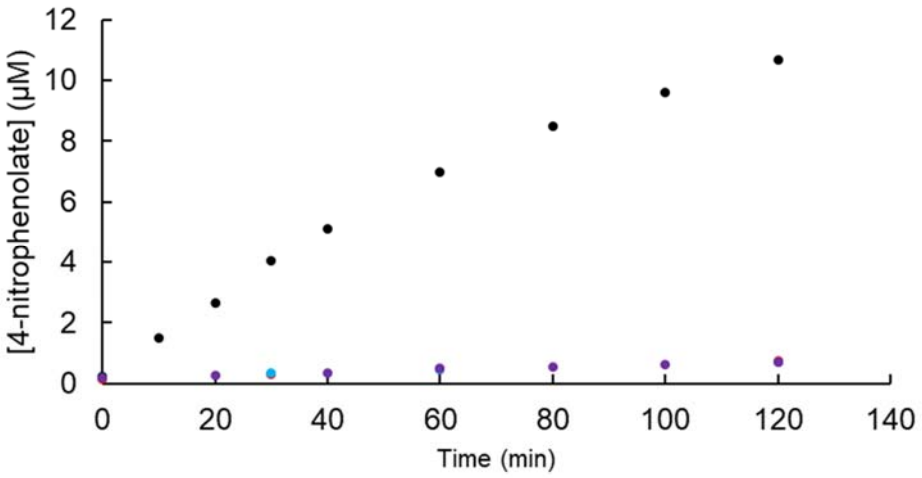

Figure S23. Hydrolysis of dimethyl *p*-nitrophenylphosphate (DMNP) in the presence of cation exchange resins. Two commercially available cation exchange resins were used to compare their activity towards hydrolysis of DMNP against **Zr-polyV$_6$**. Dowex 50WX8-100-H$^+$ ion exchange resin (●) and Amberlite IRC86-H$^+$ (●) were used under the same conditions as the **Zr-polyV$_6$** experiments in Figure 4. **Zr-polyV$_6$** (●) and control experiments (●) are also shown. The cation exchange resins demonstrate negligible hydrolytic activity under these conditions.

Video S1. **Real-time swelling of TBA-polyV$_6$ particles**. Uploaded as a separate attachment.
Video was obtained using a Leica DM4500B bright-field microscope equipped with a COHU solid state CCD camera. A 10X objective lens was used. The **TBA-polyV$_6$** powder was inserted into a 2mm-diameter capillary tube. DMF was added to the tube during video capture. Particle size analysis was conducted using IDL routines.[5]

Video S2. Swelling of TBA-polyV$_6$ after exposure to DMSO. Uploaded as a separate attachment.
Videos were obtained using an Apple iPhone and were processed using Adobe Premiere software. Video is real-time addition of 500mL of dimethyl sulfoxide to a sample of **TBA-polyV$_6$**. DMSO swells the gel upon contact, preventing the liquid from penetrating through the solid powder.

Results and Discussion

Additional characterization

Powder X-ray diffraction conducted on a sample of **TBA-polyV$_6$** shows peaks with maxima at 11.41 Å and 3.87 Å, which correspond to local ordering of V_6 clusters, as anticipated in a material composed of linked V_6 units (Figure S11).

To confirm our assignments of the ^{13}C solid-state NMR spectrum for **TBA-polyV$_6$**, we obtained spectra with and without dipolar dephasing to determine which carbon peaks are attached to protons, allowing us to distinguish between the methylene carbon and quaternary carbon in the triol units of **trisBTA** (Figure S12).

We used deconvolution of ^{13}C NMR and XPS data to obtain additional information about the structure of the polymer material. Quantitative ^{13}C solid-state NMR was conducted without cross-polarization to determine the relative peak areas. Deconvolution of these peaks estimates a ratio of 3 hexavanadate-bound to 2 unbound methylene carbons (Figure S3). Singly-capped V_6 units are unstable, meaning that each POM is found in its doubly-capped form, confirmed by the presence of a single ^{51}V NMR peak. The theoretical limit assuming only monomers is 1 bound methylene: 2 unbound methylene, whereas a linear polymer with alternating V_6 and **trisBTA** units reaches a theoretical ratio of 2 bound methylene: 1 unbound methylene. The polymer can therefore not simply be composed of linear strands and must adopt a complex structure. Deconvolution of the carbon and nitrogen peaks obtained from XPS data determined a ratio of 1.1 V_6 units per **trisBTA** linker (Figure S4). Theoretically, an infinite 2-dimensional polymer of V_6 units and linker molecules reaches an upper limit of 1.5 V_6: 1 **trisBTA**, a monomer would have a ratio of 0.5 V_6: 1 **trisBTA**, and an infinitely long linear polymer would achieve a ratio of 1 V_6: 1 **trisBTA**. A V_6: trisBTA ratio higher than 1:1 signifies that there are points where a triply-bound linker is creating a closed loop in the polymer. The observed 1.1 V_6: 1 t**risBTA** ratio for **TBA-polyV$_6$** therefore indicates the presence of roughly 9% closed-loop points in the network. Each closed loop requires two triply-bound linkers, so 18% represents a minimum estimate of the number of triply-bound linkers in the material (Fig. 2d). By compiling the molecular weight estimate from SLS, the ratio of bound linkers to unbound linkers from solid-state ^{13}C NMR, and elemental ratios obtained by both NMR and XPS we can infer that **TBA-polyV$_6$** is a cross-linked polymer with a complex non-linear structure.

To obtain an average molecular weight estimate, static light scattering (SLS) measurements conducted on a dispersion of **TBA-polyV$_6$** in DMF/H_2O determined the average molecular weight to be 1600 kDa (Figure S13) indicating the average polymer is comprised of roughly 1,000 monomer units. However, due to low solubility, this molecular weight determination can only be a rough approximation of the average molecular weight, and represents a low estimate.

Gelation behavior

The primary gelation mechanism in 1,3,5-benzenetricarboxamide-based gels is the formation of hydrogen-bonding networks.[12, 13] ATR FT-IR studies of **TBA-polyV$_6$** demonstrate a red shift in the amide 1 band of DMF from 1661 cm^{-1} to 1652 cm^{-1} upon addition of **TBA-polyV$_6$**, indicative of hydrogen bonding interactions between the gelator and the carbonyl oxygen of DMF (Figure S6). Several reports suggest that OP agents interact significantly with hydrogen-bond donors through interactions with the phosphoryl oxygen.[12, 14, 15] Pore-filling by the solvent in the cross-linked polymer is also likely to contribute to the gel formation behavior of **TBA-polyV$_6$**.

Catalysis

Our group has investigated several POM-based sulfoxidation systems, which are referenced here for the reader's convenience.[16-20]

The color change in **TBA-polyV$_6$** during the aerobic oxidation of sulfides was investigated. The yellow color when the material is diespersed in DMF is reflective of the oxygen-to-metal charge transfer absorption manifold of a fully-oxidized $[V^{V}_6O_{13}(OR)_6)]^{2-}$ core (R = **trisBTA** linkers). Upon reduction of the POM, **TBA-polyV$_6$** becomes dark green as a broad peak between 600 and 900 nm increases, attributed to intervalence charge-transfer bands in the reduced POM.[21] The persistent observation of a green reduced hexavanadate species during the course of the reaction indicates that reoxidation of **TBA-polyV$_6$** by O_2 is rate-limiting under these conditions and demonstrates the colorimetric detection capabilities of the polymer material (Figure S9).

The oxidation of propane thiol is significantly enhanced by the addition of hydrogen peroxide. Adding a 1:1 ratio of hydrogen peroxide to propane thiol results in very rapid conversion to the disulfide product both in the presence and absence of **TBA-polyV$_6$**, faster than the timescale of the experiments capable of being observed using a gc instrument. We therefore focused primarily on aerobic oxidation of thiols, which represents a more significant ideal in decontamination/deodorization applications.

When investigating the hydrolytic activity of **TBA-polyV$_6$** towards DECP, we wanted to determine whether the monomeric units would demonstrate activity and if this activity would be retained in the polyeric material. Both trials using **trisBTA** and the monomer **NH$_2$V$_6$** show hydrolytic rate enhancements (Fig. S14). These data suggest that both the linker and the hexavanadate core are contributing to catalyzing the hydrolysis of the OP analogue, and that the incorporation of these units into the heterogeneous polymer retains their catalytic activity. Additionallly, it should be noted that the hydrolysis of DECP produces HCN, so caution should be employed when using this G-agent analogue.

After substitution of TBA^+ for tetrameric zirconium hydroxide to form **Zr-polyV$_6$**, we wanted to ensure that the reaction was truly heterogeneous. A sample of **Zr-polyV$_6$** was stirred in NEM buffer at pH 10.00 for two hours, followed by filtration using a 2 µm syringe filter to remove the solid

material. The supernatant was found to have negligible catalytic activity, confirming that **Zr-polyV$_6$** catalyzes the hydrolysis as a solid material (Figure S15).

Author Contributions

The manuscript was written through contributions of all authors. All authors have given approval to the final version of the manuscript.

References

1. B. M. Fung, A. K. Khitrin and K. Ermolaev, *Journal of Magnetic Resonance*, 2000, **142**, 97-101.
2. D. A. Torchia, *Journal of Magnetic Resonance (1969)*, 1978, **30**, 613-616.
3. C. R. Morcombe and K. W. Zilm, *Journal of Magnetic Resonance*, 2003, **162**, 479-486.
4. H. Eckert and I. E. Wachs, *The Journal of Physical Chemistry*, 1989, **93**, 6796-6805.
5. J. C. Crocker and D. G. Grier, *Journal of Colloid and Interface Science*, 1996, **179**, 298-310.
6. V. W. Day, W. G. Klemperer and D. J. Maltbie, *Journal of the American Chemical Society*, 1987, **109**, 2991-3002.
7. D. Li, J. Song, P. Yin, S. Simotwo, A. J. Bassler, Y. Aung, J. E. Roberts, K. I. Hardcastle, C. L. Hill and T. Liu, *Journal of the American Chemical Society*, 2011, **133**, 14010-14016.
8. B. A. Hernandez, V. Chang, I. Villanueva and M. D. Heagy, *Journal of Organic Chemistry*, 1999, **64**, 6905-6906.
9. P. Wu, J. Chen, P. Yin, Z. Xiao, J. Zhang, A. Bayaguud and Y. Wei, *Polyhedron*, 2013, **52**, 1344-1348.
10. C. Wilson, M. Main, N. Cooper, M. E. Briggs, A. I. Cooper and D. Adams, *Polymer Chemistry*, 2017, DOI: 10.1039/C7PY00040E.
11. P. Hiemenz and R. Rajagopalan, *Journal*, 1997.
12. M. R. Sambrook and S. Notman, *Chemical Society Reviews*, 2013, **42**, 9251-9267.
13. S. Cantekin, T. F. A. de Greef and A. R. A. Palmans, *Chemical Society Reviews*, 2012, **41**, 6125-6137.
14. A. Barba-Bon, A. M. Costero, M. Parra, S. Gil, R. Martínez-Máñez, F. Sancenón, P. A. Gale and J. R. Hiscock, *Chemistry – A European Journal*, 2013, **19**, 1586-1590.
15. M. R. Sambrook, J. R. Hiscock, A. Cook, A. C. Green, I. Holden, J. C. Vincent and P. A. Gale, *Chemical Communications*, 2012, **48**, 5605-5607.
16. J. W. Han, K. I. Hardcastle and C. L. Hill, *European Journal of Inorganic Chemistry*, 2006, **2006**, 2598-2603.
17. J. W. Han and C. L. Hill, *Journal of the American Chemical Society*, 2007, **129**, 15094-15095.
18. C. L. Hill, T. M. Anderson, J. W. Han, D. A. Hillesheim, Y. V. Geletii, N. M. Okun, R. Cao, B. Botar, D. G. Musaev and K. Morokuma, *Journal of Molecular Catalysis A: Chemical*, 2006, **251**, 234-238.
19. Y. Hou and C. L. Hill, *Journal of the American Chemical Society*, 1993, **115**, 11823-11830.
20. N. M. Okun, T. M. Anderson and C. L. Hill, *Journal of the American Chemical Society*, 2003, **125**, 3194-3195.
21. Q. Chen, D. P. Goshorn, C. P. Scholes, X. L. Tan and J. Zubieta, *Journal of the American Chemical Society*, 1992, **114**, 4667-4681.